JOURNAL OF CATALYSIS 96, 12–22 (1985)

Sintering Behavior of Nickel Particles Supported on Alumina Model Catalyst in Hydrogen Atmosphere

KYONG-TAE KIM AND SON-KI IHM[1]

Department of Chemical Engineering, Korea Advanced Institute of Science and Technology, P.O. Box 150 Chongyangni, Seoul 131, Korea

Received December 12, 1984; revised April 9, 1985

The sintering behaviors under hydrogen at 600, 700, and 800°C of nickel crystallites supported on the anodic alumina film were investigated through transmission electron microscopy. The prevailing mode of sintering at 600 and 700°C is believed to be due to the particle migration and that at 800°C is due to the atomic migration or Ostwald ripening. The shift of the sintering mechanism at 800°C was deduced in terms of the interaction of nickel with alumina, rather than in terms of the effect from the porous surface proposed by Kuo *et al.* (*J. Catal.* **64**, 303, 1980). It was also found that very large faceted nickel crystallites were formed locally for the specimens heated at 800°C.

INTRODUCTION

In the supported–metal catalysts, the phenomenon termed sintering or aging occurs with use or treatment for long periods at elevated temperatures. The occurrence of sintering results in the decrease of the exposed surface area of metal, which changes the activity and sometimes the selectivity of these catalysts. Therefore, the investigations on the process by which sintering occurs have been extensively performed both theoretically and experimentally. Sintering has been considered to occur by at least two different mechanisms, that is, particle migration and atomic migration. The particle migration mechanism (*1, 2*) includes migrations of particles on support, collisions between the particles, and their coalescences. The atomic migration mechanism (*3, 4*), often called Ostwald ripening (*5*), includes transport of atomic (or molecular) units. These two mechanisms are believed to occur simultaneously. However, the prevailing mechanism could not easily be determined because the sintering process is affected by various factors, including the temperature, the time, the chemical atmosphere, and the nature of support.

The change of particle size distribution (PSD) can be considered as a direct measure to the rate of sintering (*6, 7, 8*). The kinetics of sintering has been expressed as

$$\frac{dS}{dt} = -KS^n, \qquad (1)$$

where S is the exposed surface area of metal per unit area of support, and n is the sintering exponent which can be predicted between 4 and 8 for a particle migration mechanism and from <2 to >13 for an atomic migration mechanism. On the other hand, the direct observation of metal particles may provide some clear evidence of the sintering process. This is favorably done with transmission electron microscopy (TEM). With TEM, the selected area of a specimen can be examined after each heat treatment. Usually a model catalyst used, which is made up of a thin layer of support upon which metal particles are deposited.

In the present work, the sintering behaviors of Ni/alumina model catalyst were investigated under hydrogen atmosphere in

[1] To whom all correspondence should be addressed.

0021-9517/85 $3.00

view of its wide industrial applications as in methanation and hydrogenation. Even if the nickel particles on alumina are notorious for their poor TEM images compared with other metal–support combinations (*9*), the measurements can be made quite accurately except for very small particles (below about 2 nm in diameter). The aims of the present work are to observe the sintering phenomena with TEM and to propose the predominant mechanism for the nickel supported on alumina model catalyst.

EXPERIMENTAL PROCEDURES

Anodization and sputtering. The alumina supports were prepared by the method described in Ref. (*10*). Anodic oxidation of aluminum foil was carried out in a 3 wt% solution of tartaric acid at 15 V for 20 sec. The nonporous and amorphous aluminum oxide film thus prepared was considered to be about 250 Å thick since the anodizing velocity is about 15 Å/V (*11*). The amorphous alumina films were picked up on gold grids, and some were calcined in air at 620°C for 40 hr and transformed into the crystalline γ-phase. These amorphous alumina and γ-alumina supports were coated with nickel by the sputtering technique in a Mini-Coater (Fullam Co.). To obtain the initially identical specimens for measuring the particle size distribution, several alumina supports were placed together in the Mini-Coater and sputtered under the same condition.

Heat treatment. The model catalysts thus prepared were subjected to heat treatment in hydrogen atmosphere for various lengths of time and at temperatures of 600, 700, and 800°C. All the sintering experiments were performed in a quartz tube located inside a tubular furnace. The specimens were placed into the middle section of the tube, and helium gas (99.999%) was allowed to flow through until the specimens were heated to the desired temperature. As

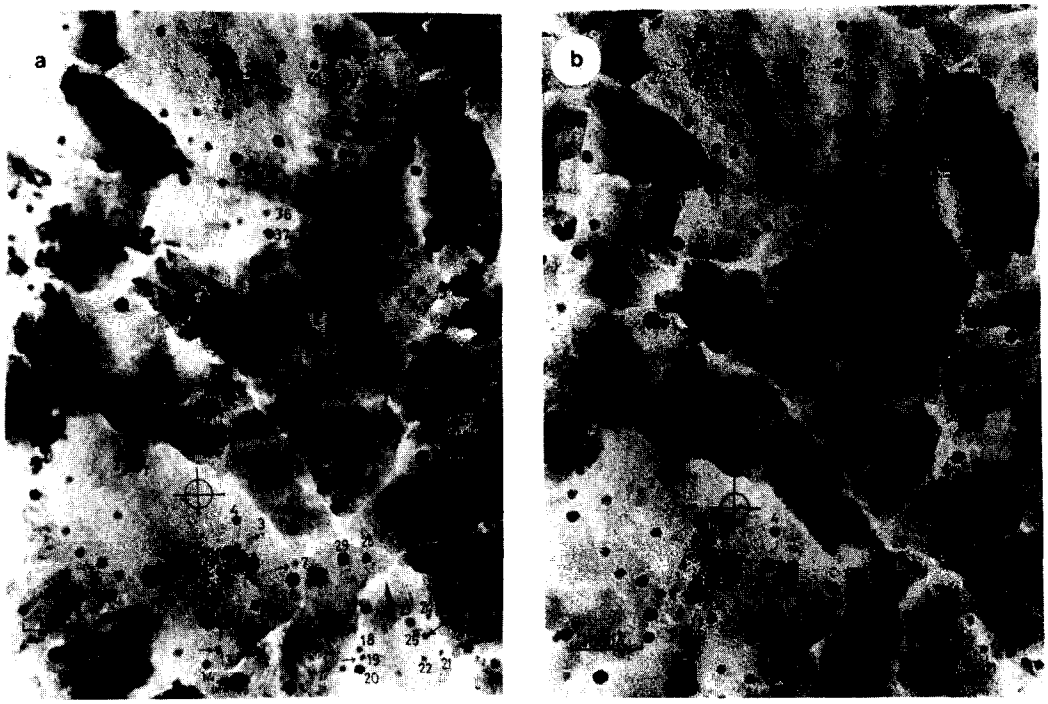

FIG. 1. Electron micrographs for the same region of Ni/γ-alumina model catalysts heated in H_2 at 700°C for (a) 5 and (b) 6 hr. The arrows in (a) indicate the particles that disappeared in the next step, and the numbers indicate particular particles of interest.

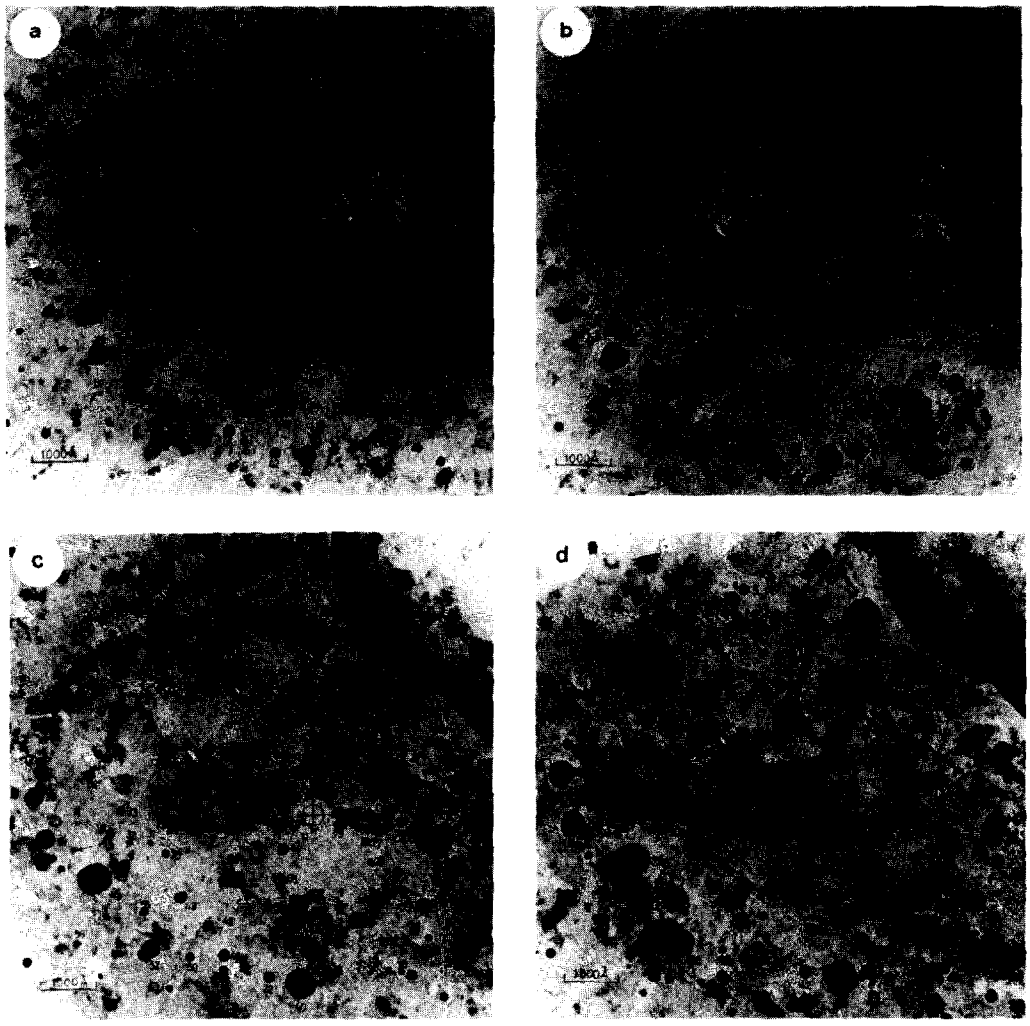

FIG. 2. Electron micrographs for the same region of Ni/γ-alumina model catalysts heated in H_2 at 800°C for (a) 5.5, (b) 6, (c) 6.5, and (d) 7.5 hr. The arrows indicate the particles that disappeared in the next step, and the numbers indicate particular particles of interest.

soon as the chosen temperature was reached, helium was replaced by hydrogen. The flow rate of hydrogen was 40 ml(STP)/min. After heating for the desired period of time, the gas was again replaced by helium and the specimens were cooled to room temperature.

TEM Observations. The transmission electron microscope used was JEOL (JEM100CX), and the accelerating voltage applied was 100 kV. The same region of a specimen was observed after each heat treatment to follow the changes in size, shape, and position of individual particles. Two or three areas were selected for each specimen to decide the size distribution and the average size as a function of time and temperature. It should be noted that the TEM samples were exposed to atmosphere and that observations were made on the nickel particles in the oxide state.

RESULTS

1. Behavior of Individual Particles

Figures 1 and 2 show the transmission electron micrographs of the same region of

TABLE 1

Schematic Illustrations of Various Events Observed on the Electron Micrographs (Figs. 1a and b) during the Heat Treatment, and of Possible Mechanisms

Before (5 hr)	After (6 hr)	Possible mechanisms
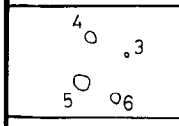	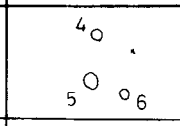	particle migration or Ostwald ripening
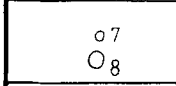	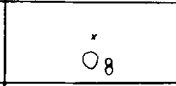	particle migration or Ostwald ripening
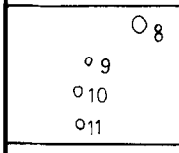	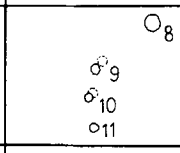	particle migration
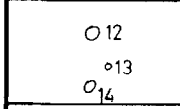	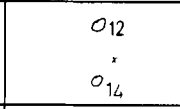	particle migration or Ostwald ripening
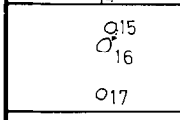	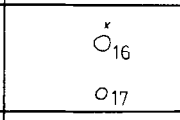	particle migration or Ostwald ripening
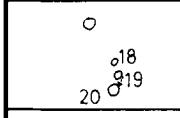	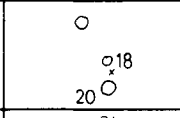	particle migration or Ostwald ripening
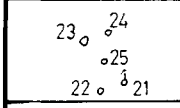	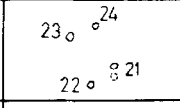	particle migration or Ostwald ripening
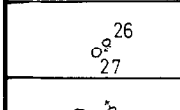	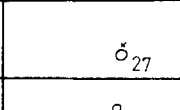	particle migration or Ostwald ripening
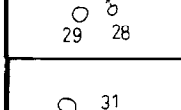	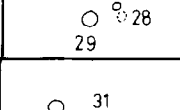	particle migration
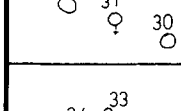	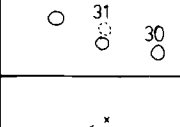	particle migration
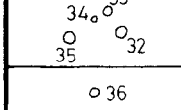	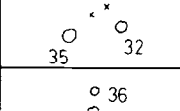	particle migration or Ostwald ripening
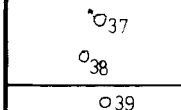	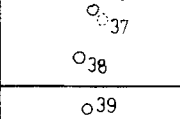	particle migration
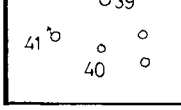	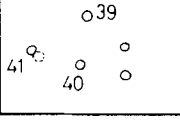	particle migration

Note. The dashed arrows indicate the possible direction of particle migration or Ostwald ripening, and the crosses indicate the original position of the particles that have disappeared.

a specimen heated to 700 and 800°C, respectively. Relative movement of individual grains of the alumina support occurred during treatment, and the relative positions of Ni particles on individual Al_2O_3 grains remained essentially unaltered. However, various local events for some of the Ni particles, migration and/or disappearance, were observed on the electron micrographs and are listed in Tables 1 and 2.

At 700°C, both the disappearance and migration of Ni particles occurred. For example, the small particles of 30 to ~100 Å (particles 3, 7, 13, 15, 19, 25, 26, 33, and 34 in Fig. 1a) disappeared after being heated for 1 hr. The disappearance of a Ni particle is possible not only by the atomic migration through Ostwald ripening but also by the particle migration. Particles of about 70 Å (particles 9, 21, and 28 in Fig. 1a) to about 120 Å (particles 31, 37, and 41 in Fig. 1a) were found to be able to migrate a distance up to about 150 Å, which are the direct evidences to the particle migration mechanism.

At 800°C, on the other hand, small parti-

TABLE 2

Schematic Illustrations of Various Events Observed on the Electron Micrographs (Figs. 2a–d) during the Heat Treatment, and of Possible Mechanisms

Before (5.5 hr)	After (6 hr)	Possible mechanisms
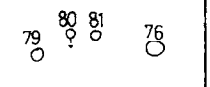	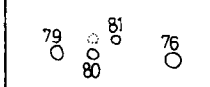	particle migration
Before (6 hr)	After (6.5 hr)	possible mechanisms
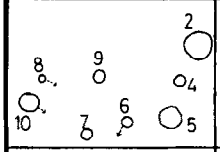	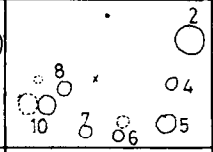	particle migration or Ostwald ripening
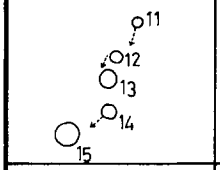	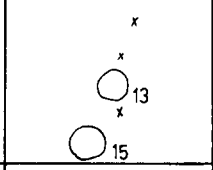	particle migration or Ostwald ripening
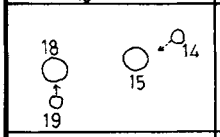	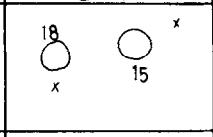	particle migration or Ostwald ripening
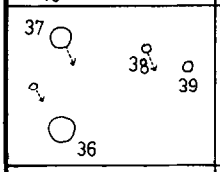	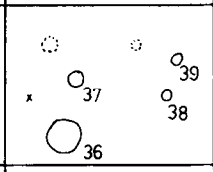	particle migration or Ostwald ripening
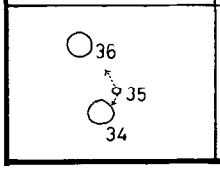	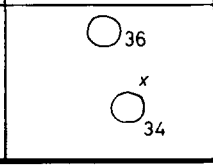	particle migration or Ostwald ripening

Note. The dashed arrows indicate the possible direction of particle migration or Ostwald ripening, and the crosses indicate the original position of the particles that have disappeared.

TABLE 2—*Continued*

Before (6 hr)	After (6.5 hr)	Possible mechanisms
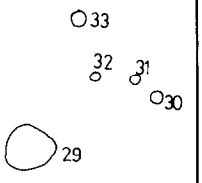	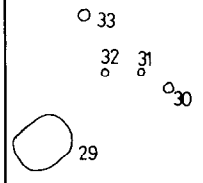	Ostwald ripening
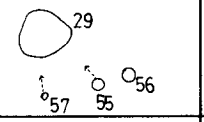	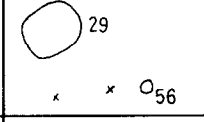	particle migration or Ostwald ripening
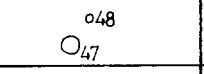	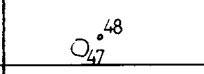	Ostwald ripening
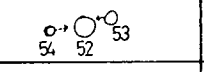	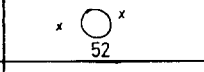	particle migration or Ostwald ripening
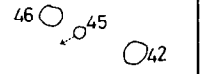	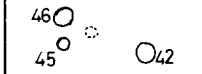	particle migration
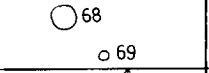	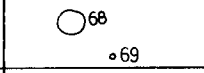	Ostwald ripening
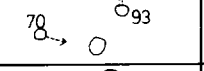	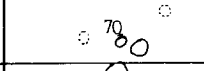	particle migration
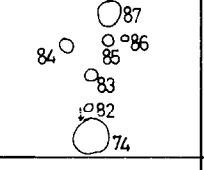	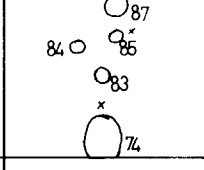	particle migration or Ostwald ripening
Before (6.5 hr)	After (7 hr)	
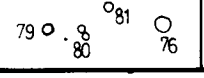	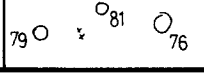	particle migration or Ostwald ripening

cles were frequently found not only to disappear but also to become smaller during heating. For example, particles 11 and 12 in Fig. 2b of about 150 Å in diameter disappeared after heating for 0.5 hr, probably captured by particle 13 through the particle migration or the atomic migration mechanism. The same can be said for particles 14, 19, 35, 53–55, 57, 80, and 82 as shown in Table 2. Particles 31, 32, 48, and 69 were found to become considerably smaller in size, and this phenomenon must be interpreted as clear evidence to the metal growth by the atomic migration mechanism (*12*). Also, at 800°C the migration of particles (for example, particles 45 and 70) frequently occurred, indicating the particle migration mechanism. Large particles (for example, particles 1, 27, 29, 40, and 74 in Fig. 2) were faceted and significantly increased in size during heating at 800°C. It should also be noted that the smaller particles less than 20 Å in size are not detected due to the resolution limit of TEM and that the amount of such smaller particles can be considerable. This can be evidenced by the fact that most particles in Fig. 1b are somewhat larger than those in Fig. 1a.

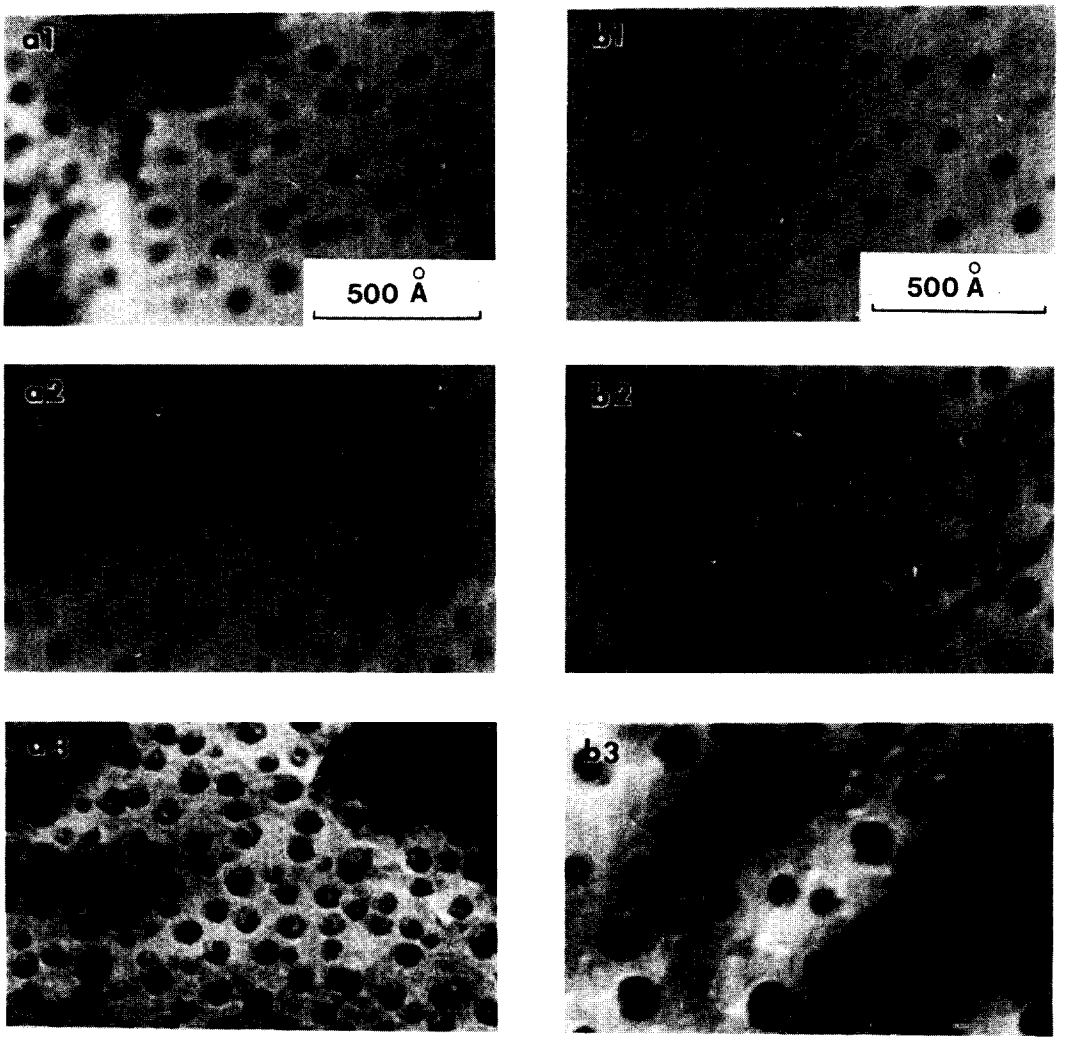

FIG. 3. Electron micrographs of Ni/γ-alumina model catalyst heated in H_2 (a) at 700°C for (a1) 10, (a2) 20, and (a3) 41 hr; and (b) at 800°C for (b1) 10, (b2) 20, and (b3) 43 hr.

2. Particle Size Distribution (PSD)

Figures 3a and b show the electron micrographs of Ni/γ-alumina model catalysts heated at 700 and 800°C, respectively. About 600 to 1000 particles were counted to measure the particle sizes. Table 3 is a summary of the effect of experimental conditions on the average particle size of Ni/γ-alumina model catalysts. The geometric mean diameter, $\bar{D}_g$, is defined as $\ln \bar{D}_g = \Sigma_i N_i \ln \bar{D}_i (\Sigma_i N_i)^{-1}$, and geometric standard deviation, σ_g, $\ln \sigma_g = [\Sigma_i N_i (\ln D_i - \ln \bar{D}_g)^2 (\Sigma_i N_i)^{-1}]^{1/2}$, in which N_i is the number of particles with diameters between $\bar{D}_i - \Delta D_i/2$ and $\bar{D}_i + \Delta D_i/2$; $\bar{D}_i$ is the average diameter in each diameter interval. Kuo and De Angelis (*13*) used the geometric mean diameter for the particle size and explained the increase of standard deviation with time as a possible indicator of change in the sintering mechanism at a higher temperature. In Table 3, the similar trend is found at 800°C. Figure 4 shows the histograms of the particle size distributions under each experimental condition. To see the effect of tem-

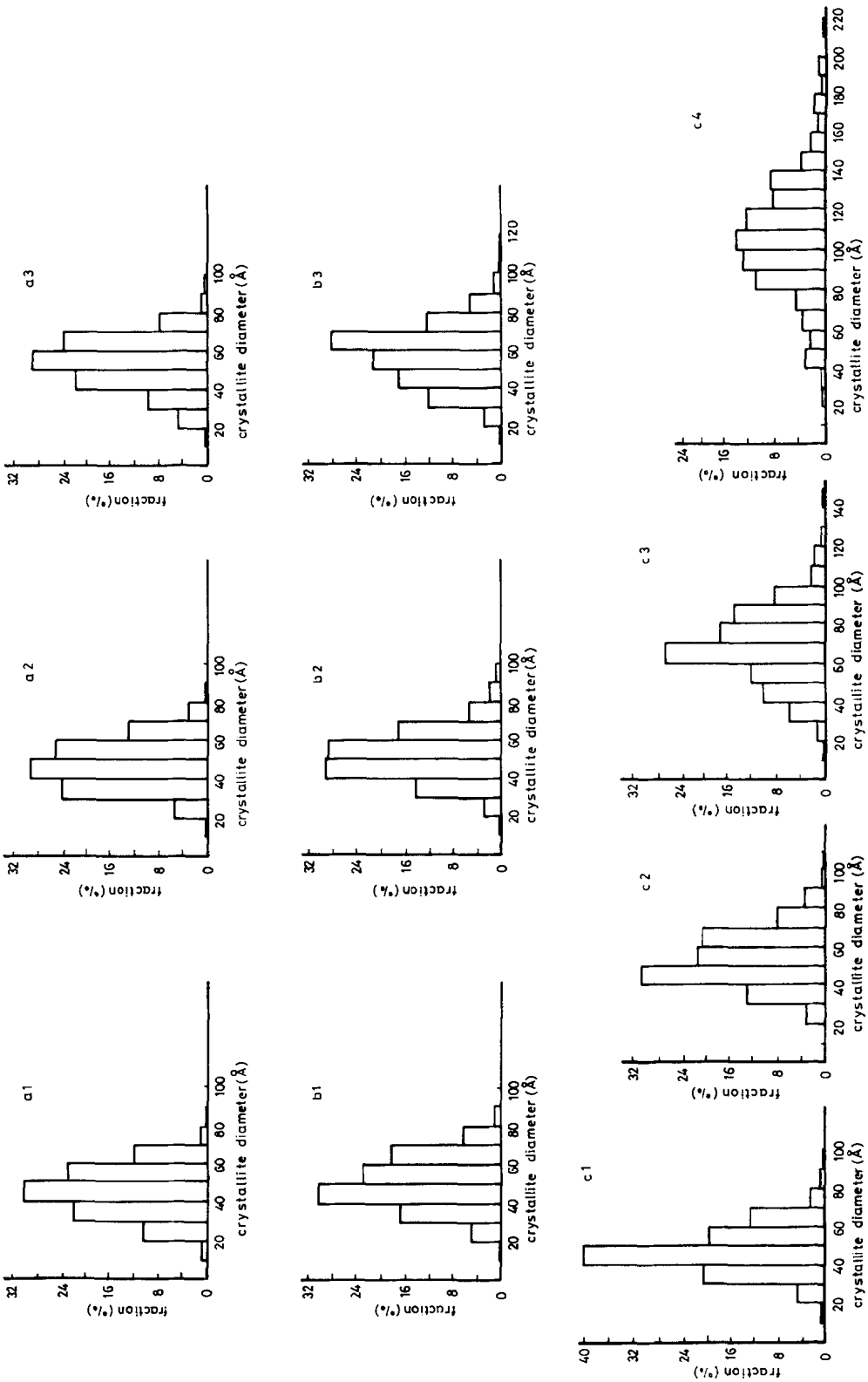

FIG. 4. Histograms of particle size distributions of Ni/γ-alumina model catalyst heated in H_2 at 600°C for (a1) 10, (a2) 20, and (a3) 45 hr; (b) at 700°C for (b1) 10, (b2) 20, and (b3) 41 hr; and (c) at 800°C for (c1) 5, (c2) 10, (c3) 20, and (c4) 43 hr.

TABLE 3

Effect of Experimental Conditions on the Sintering of Ni/γ-Alumina Model Catalysts

Treatment conditions		Time (hr)	Geometric mean diameter, D_g (Å)	Geometric standard deviation, σ_g
Atmosphere	Temperature (°C)			
H_2	600	10	44.0	1.34
H_2	600	20	46.4	1.30
H_2	600	45	52.4	1.33
H_2	700	10	49.2	1.32
H_2	700	20	50.4	1.30
H_2	700	41	55.7	1.34
H_2	800	5	46.0	1.32
H_2	800	10	51.6	1.34
H_2	800	20	65.0	1.37
H_2	800	43	104.0	1.39

perature on the PSDs, the approximate curves drawn from Fig. 4 were compared at a given time, as shown in Fig. 5. The PSDs at 600 and 700°C remained nearly unchanged, while at 800°C they were considerably shifted to the larger sizes of the distribution. On heating for up to 20 hr, the PSD did not show any detectable changes, but after 40 hr it was remarkably broadened at 800°C. The effect of time on PSD can also be evidenced from Fig. 6, and it is seen to be the most significant at 800°C. It is noted that the electron micrograph in Fig. 7 shows the abnormal growth phenomenon

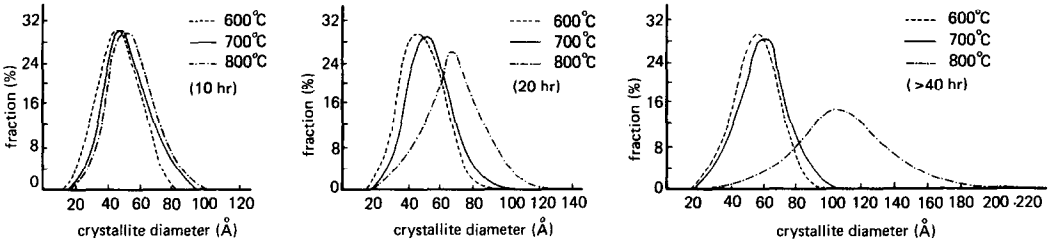

FIG. 5. Comparison of particle size distributions of Ni/γ-alumina model catalyst heated in H_2 at 600, 700, and 800°C for 10, 20, and more than 40 hr, respectively, showing the effect of temperature (reconstructed from Fig. 4).

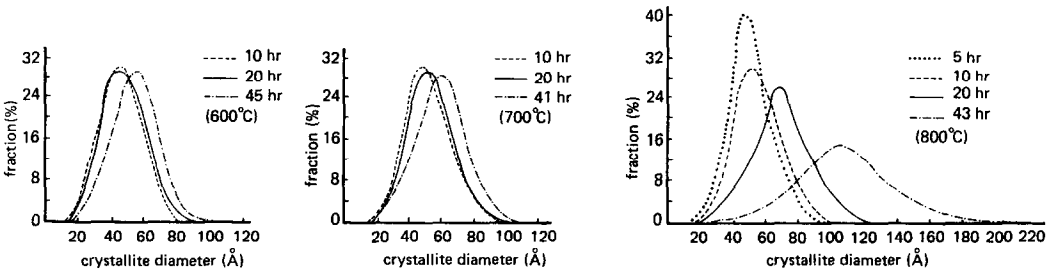

FIG. 6. Comparison of particle size distributions of Ni/γ-alumina model catalysts heated in H_2 for 10, 20, and more than 40 hr at 600, 700, and 800°C, respectively, showing the effect of heating duration (reconstructed from Fig. 4).

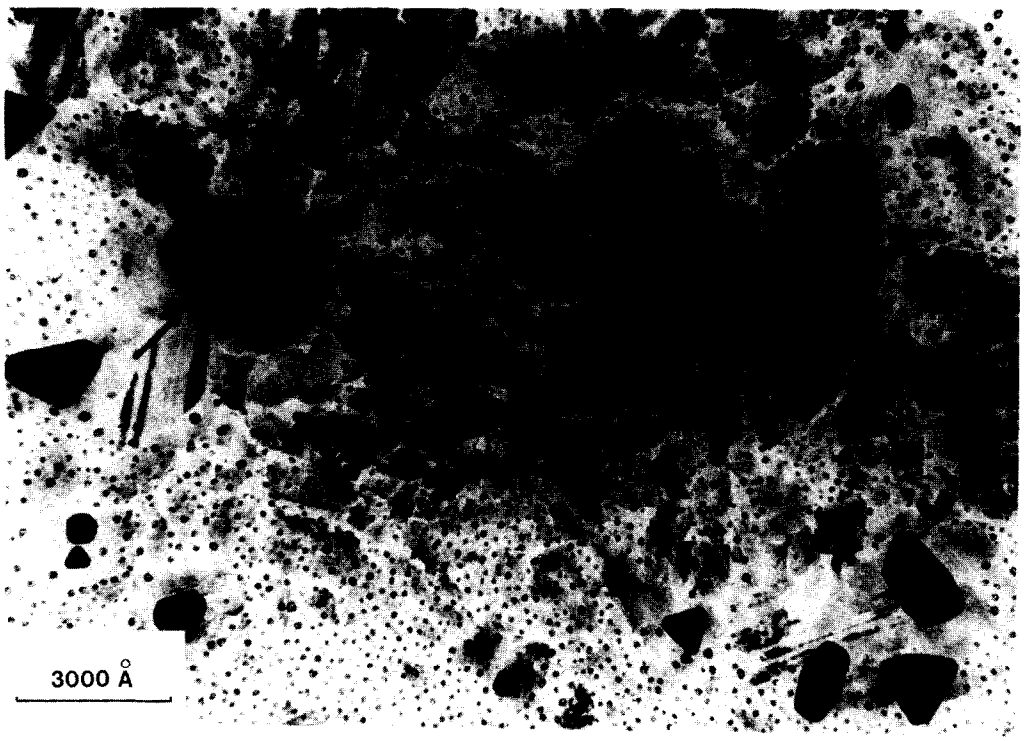

FIG. 7. Electron micrograph of Ni/γ-alumina model catalyst heated in H_2 at 800°C for 43 hr (the same as in Fig. 3-b3). The large faceted crystallites are shown to appear.

(*14*) existed locally in the same specimen of Fig. 3-b3, heated at 800°C for 43 hr. The appearance of the large, faceted particles may be a similar phenomenon to that shown in Fig. 2.

3. *Sintering Rate*

The power-law-type Eq. (1) was employed to explain the sintering rate. Equation (1) can be rewritten as

$$\left(\frac{\bar{D}}{\bar{D}_0}\right)^m = 1 + \alpha t, \qquad (2)$$

where α is a constant, $\bar{D}$ and $\bar{D}_0$ are the average particle diameters at time t and 0, respectively, and $m + 1$ is the sintering exponent n. If the value of αt is much larger than unity, the sintering exponent can be found from the slope in the plot of log $\bar{D}$ vs log t. The criterion of $\alpha t \gg 1$ cannot be checked at this moment. Moreover, the initial condition of $t = 0$ for the power-law equation may be arbitrary, especially if the sintering mode varies with time.

Kuo *et al.* (*15*) studied the sintering of the nickel/silica commercial catalyst and, following Wynblatt and Gjostein (*16*) without discussing the condition of $\alpha t \gg 1$, plotted their data in the coordinate of log $(\bar{D}/\bar{D}_0)$ vs log t. For comparison with their work, the present data were also plotted in a similar manner in Fig. 8. The sintering exponent n at 600 and 700°C are 10.5 and 12, respectively, while n at 800°C is 3. This change of n value observed in this investigation is very similar to the results obtained by Kuo *et al.* (*15*).

Their sintering exponent n in hydrogen atmosphere changed from 14 to 4 with the temperature varying from 700 to 800°C. They proposed that sintering predominantly occurs by a particle migration mechanism at temperatures of 700°C and below

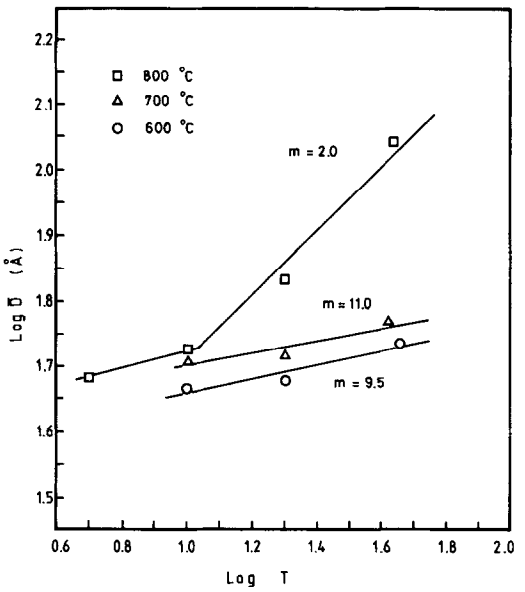

FIG. 8. Plot of log $\bar{D}$ vs log t for Ni/γ-alumina model catalyst heated in H_2 atmosphere.

and by an atomic migration mechanism at 800°C. Recently, Nakayama *et al.* (*17*) showed that the prevailing mechanism in hydrogen at 600°C was particle migration on Al_2O_3 but atomic migration on SiO_2. They postulated that a strong nickel/alumina interaction is formed only at high temperatures and also a nickel–aluminate complex would be formed at higher temperatures than nickel silicate.

DISCUSSION

Two mechanisms were clearly responsible for the growth of nickel particle on alumina model catalyst. The sintering characteristics at 800°C in the present work by using TEM are (1) the direct evidence to the Ostwald ripening, which was not observed at 700°C, (2) the formation of very large faceted crystallites, (3) the broadening of PSD, and (4) the substantial decrease in the sintering exponent. If it is reasonably accepted that the abrupt change of the sintering exponent implied the change of the sintering mechanism, the predominant mode of sintering is shifted from the particle migration to the atomic migration with the temperature changing from 700 to 800°C. Because the present model catalyst is of flat geometry, the effect of pore structure on this shift suggested by Kuo *et al.* (*15*) does not seem to serve the purpose. The nature of support material seems to be a rather good source of explanation. In other words, the interaction of nickel particles with alumina or the formation of nickel aluminate must be enhanced at 800°C.

ACKNOWLEDGMENTS

The TEM observations were made at the Lucky Central Research Institute, Daeduck, Korea, and the authors express sincere gratitude to Dr. Jong Kee Yeo, Mr. Jong Man Oh, and Mr. Se Ahn Song for their effective cooperation.

REFERENCES

1. Ruckenstein, E., and Pulvermacher, B., *J. AIChE.* **19,** 356 (1973).
2. Ruckenstein, E., and Pulvermacher, B., *J. Catal.* **29,** 224 (1973).
3. Flynn, P. C., and Wanke, S. E., *J. Catal.* **34,** 390 (1974).
4. Flynn, P. C., and Wanke, S. E., *J. Catal.* **34,** 400 (1974).
5. Ruckenstein, E., and Dadyburjor, D. B., *Thin Solid Films* **55,** 89 (1978).
6. Granqvist, C. G., and Buhrman, R. A., *J. Appl. Phys.* **47,** 2200 (1976).
7. Granqvist, C. G., and Buhrman, R. A., *J. Catal.* **42,** 477 (1976).
8. Granqvist, C. G., and Buhrman, R. A., *J. Catal.* **46,** 238 (1977).
9. Mustard, D. G., and Bartholomew, C. H., *J. Catal.* **67,** 186 (1981).
10. Ruckenstein, E., and Malhotra, M. L., *J. Catal.* **41,** 303 (1976).
11. Diggle, J. W., Downie, T. C., and Goulding, C. W., *J. Chem. Rev.* **69,** 365 (1969).
12. Chen, J. J., and Ruckenstein, E., *J. Catal.* **69,** 254 (1981).
13. Kuo, H. K., and De Angelis, R. J., *J. Catal.* **68,** 203–207 (1981).
14. Wynblatt, P., and Gjostein, N. A., *Acta Metall.* **24,** 1175 (1976).
15. Kuo, H. K., Ganesan, P., and De Angelis, R. J., *J. Catal.* **64,** 303 (1980).
16. Wynblatt, P., and Gjostein, N. A., *Scr. Metall.* **9,** 969 (1973).
17. Nakayama, T., Arai, M., and Nishiyama, Y., *J. Catal.* **87,** 107 (1984).